

Branched Aramid Nanofibers

Jian Zhu, Ming Yang, Ahmet Emre, Joong Hwan Bahng, Lizhi Xu, Jihyeon Yeom, Bongjun Yeom, Yoonseob Kim, Kyle Johnson, Peter Green, and Nicholas A. Kotov*

Abstract: Interconnectivity of components in three-dimensional networks (3DNs) is essential for stress transfer in hydrogels, aerogels, and composites. Entanglement of nanoscale components in the network relies on weak short-range intermolecular interactions. The intrinsic stiffness and rod-like geometry of nanoscale components limit the cohesive energy of the physical crosslinks in 3DN materials. Nature realizes networked gels differently using components with extensive branching. Branched aramid nanofibers (BANFs) mimicking polymeric components of biological gels were synthesized to produce 3DNs with high efficiency stress transfer. Individual BANFs are flexible, with the number of branches controlled by base strength in the hydrolysis process. The extensive connectivity of the BANFs allows them to form hydro- and aerogel monoliths with an order of magnitude less solid content than rod-like nanocomponents. Branching of nanofibers also leads to improved mechanics of gels and nanocomposites.

Three-dimensional networks (3DNs) assembled from inorganic nanoscale components are known to markedly improve the mechanical, electrical, ion-transport, and other properties of composite materials.^[1] Rod-like or sheet-like nanomaterials, exemplified by carbon nanotubes (CNTs),^[2] graphene,^[3] metal or ceramic nanowires,^[4,11] or cellulose nanofibers (CellNFs),^[5] typically serve as building blocks of 3DNs. Intermolecular interactions upon their physical contact lead to formation of the extended networks, but these contacts also represent the weak links of 3DNs. Being formed by relatively

weak and short-range intermolecular interactions, the contact sites are mechanically disrupted much easier than the fibers themselves, which results in a precipitous decrease of strength, strain, and toughness. For instance, the intermolecular cohesive energy of orthogonal contacts between two single-walled CNTs is only about 2 eV, or 0.005 eV per carbon atom.^[6] In case of perfect alignment of cellulose fibers, cohesion energy is high, that is, ca. 1.9 eV per unit chain,^[7] but for orthogonal contact of CellNFs, it suffers from unoptimized orientation of hydrogen bonds, which causes a deterioration of mechanical properties.^[8] Furthermore, the negative charges associated with the oxidation of cellulose during preparation^[9] are associated with fiber–fiber repulsion, potentially curtailing the network formation in solution or requiring extra treatment.

The importance of 3DNs for load-bearing structures, energy storage devices, emerging electronics technologies, and biomaterials motivated our search for new approaches to the assembly of nanoscale components in 3DNs. As is the case for many materials with high mechanical performance, the replication of engineering approaches used in nature are worthy of consideration. The most common strategy for creation of 3DNs in living organisms is the self-assembly of protein, peptide, or polysaccharide units with repetitive Y-segments and long nanoscale branches.^[10] This strategy enables the cohesion energy of the nanofiber at the contacts to be comparable to that along the units in the protein chain. This design concept of 3DNs is used in the cytoskeletons of living cells^[11] and the extracellular polymer matrix of bacterial biofilms; both of these biomaterials are known for their high toughness and exceptional range of elasticity.^[12] Direct reproduction of 3DN assemblies will require peptide units with lock-and-key junctions and bifurcation segments. While such self-assembled networks from artificial peptides are fundamentally possible, a different and simpler approach would be preferred.

One key question is whether it is possible to have high-strength nanofibers as building blocks and increase the network-averaged cohesion energy of the contacts. A realistic pathway to such materials is to reduce the volumetric density of the weak links in 3DNs. Branched flexible nanofibers would be essential for attaining this goal because they reduce the number density of orthogonal interconnects. If the fibers are thin and flexible, the cohesion energy at the contact sites may actually increase due to entanglement. Few synthetic methods, however, are available to produce flexible and branched nanofibers that could potentially serve as the basis for 3DN components. The difficulties inherent in obtaining freely dispersible branching nanofibers can be noted across all materials platforms: carbon, cellulose, ceramics, metals, and others. In some cases, this is related to the limitations of their

[*] Prof. Dr. J. Zhu, Prof. Dr. M. Yang, A. Emre, J. H. Bahng, Dr. L. Xu, J. H. Yeom, Dr. B. J. Yeom, Dr. Y. S. Kim, Prof. Dr. N. A. Kotov
Department of Chemical Engineering, University of Michigan
Ann Arbor, 48109 (USA)
E-mail: kotov@umich.edu


Prof. Dr. J. Zhu
School of Materials Science and Engineering, Nankai University
Tianjin, 300350 (China)

Prof. Dr. M. Yang
Key Laboratory of Microsystems and Micronanostructures Manufacturing, Harbin Institute of Technology, Harbin, 150080 (China)

K. Johnson, Prof. P. Green, Prof. Dr. N. A. Kotov
Department of Materials Science, University of Michigan
Ann Arbor, 48109 (USA)

Prof. P. Green, Prof. Dr. N. A. Kotov
Biointerfaces Institute, University of Michigan
Ann Arbor, 48109 (USA)

Prof. Dr. N. A. Kotov
Department of Biomedical Engineering, University of Michigan
Ann Arbor, 48109 (USA)

 Supporting information and the ORCID identification number(s) for the author(s) of this article can be found under:
<https://doi.org/10.1002/anie.201703766>.

production by gas-phase catalysis (carbon fibers, nanotubes, or nanowires). In other cases, such difficulties originate from the inability to finding suitable hydrolysis conditions.

Herein, we report that branched nanofibers suitable for common building blocks for a variety of 3DNs can be prepared from microfibers of Kevlar by partial ionization of aramid chains. The resulting branched aramid nanofibers (BANFs) undergo a facile gelation processes and produce highly porous 3DNs. The shear moduli and strengths of circa 30 kPa, and 3 kPa found in BANF gels, exceed those from polymeric hydrogels^[13] or other gels made by non-branched nanofibers. The better interconnectivity and the high strength of BANF together should increase energy dissipation in 3DNs.

Kevlar macroscale fibers (KMFs) consist of aligned poly(*p*-phenylene terephthalamide) (PPTA) chains connected by intermolecular hydrogen bonds (Figure 1a). The structural hierarchy of KMFs visualized by scanning electron microscopy (SEM) after fracturing (Figure 1b,c) displays the presence of constitutive nanofibers. KMF can be split chemically into nanofibers by deprotonation with saturated KOH in dimethyl sulfoxide (DMSO).^[14] The abstraction of protons from PPTA leads to the dissociation of weaker intermolecular bonds, while the constitutive nanofibers remain intact. Atomic force microscopy (AFM) images of the BANFs indicate that they have an average diameter of 4.5 nm (Supporting Information, Figure S1), and a total length of several micrometers (Figure 1d,e). They display unusual branching morphology, which was directly evidenced by multiple experimental techniques: transmission electron microscopy (TEM), scanning electron microscopy (SEM), TEM tomography (Figure 1f,g, Supporting Information,

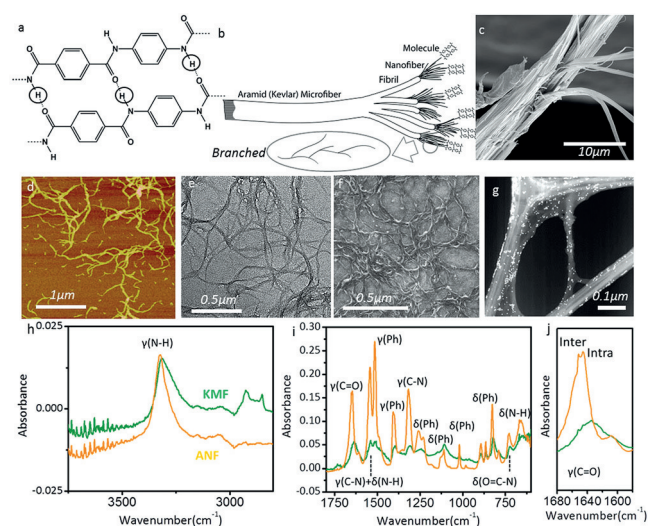


Figure 1. BANF preparation and characterization. a) Molecular structure of PPTA chains. b) The hierarchical structure of Kevlar microfibers (KMF). c) SEM image of the fractured KMF showing the fibrils and constitutive nanofibers. d) AFM image of BANFs deposited on a silicon substrate. e) TEM image showing bifurcated BANFs. f) SEM image of bifurcated BANFs. g) TEM 3D tomography image showing the 3D structure of the branch. h)–j) FTIR spectra for KMF and BANF. The stretching and bending modes of different functional groups are indicated by γ and δ , respectively.

Video S1). The ability of BANFs to branch several times along their length is likely to be a reflection of their structural organization in KMFs. Furthermore, the branching pattern can be controlled by using different bases for the deprotonation of PPTA. Potassium ethoxide (EtOK) leads to nanofibers with greater number of branches. Besides microscopy, the increased degree of branching can also be evidenced by the increased viscosity of the BANF dispersions (Supporting Information, Figure S2).

The chemical signature that differentiates the aramid nanofibers from the KMFs is the upshift of N–H and C=O stretching vibrations (Figure 1h–j) in the FTIR spectra.^[14a] The higher energy of these molecular vibrations is related to the higher average strength of hydrogen bonds in the material. The increase of the energy of the hydrogen bonds can be associated with the optimization of chain conformations in nanofibers. Interestingly, the C=O vibration mode was split into two peaks (Figure 1j), which can be attributed to intra- and inter-nanofiber hydrogen bonds.^[15] The closeness of FTIR peaks indicates that the energy of fiber-to-fiber contact points approaches that of aramid chain bonding within the fibers, which is required to eliminate weak links in 3DNs.

BANF hydrogels can be easily attained by solvent exchange (Supporting Information, Figure S3a).^[5c] In a typical procedure, a layer of deionized (DI) water is poured on top of a 1% (w/v) BANF in DMSO. The PPTA chains are gradually neutralized by seizing protons from water; this process is accompanied by a color change from dark red to light yellow (Figure 2a vs. 2b) typical of Kevlar. The differences in the mechanical properties associated with solvent exchange can be immediately noticed by the formation of the hydrogel. Unlike typical hydrogels, those from BANF are robust and can be cut with a razor blade (Figure 2c). To understand better the structure of the hydrogel, it was transformed into an aerogel through the supercritical extraction of water with liquid CO₂ (Figure 2d–f). SEM images of the aerogel revealed a network of BANF nanofibers entangled with each other. The specific density of the BANF aerogel was $\rho = 11 \text{ mg cm}^{-3}$

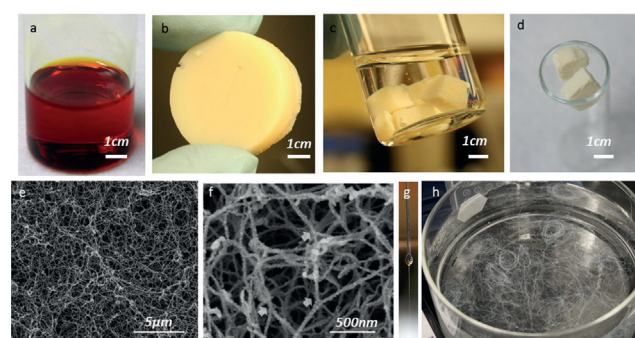


Figure 2. Fabrication of BANF hydrogels and aerogels. a) BANF dispersion in DMSO. b)–d) Photographs of b) BANF hydrogel, c) pieces of hydrogels cut and stored in fresh deionized water, d) BANF aerogels wedged in the opening of a beaker. e), f) SEM images of a BANF aerogel at different magnifications. g) Photograph of hydrogel fibers jetting from a capillary glass tube. h) Hydrogel fibers collected in a beaker.

(Figure 2d), which is comparable to or lighter than lattice metamaterials with lithographically-prepared trusses^[16] ($\rho = 6.3\text{--}258\text{ mg cm}^{-3}$). The Brunauer–Emmett–Teller (BET) surface area of the BANF aerogels was $275\text{ m}^2\text{ g}^{-1}$, which is comparable with that of graphene aerogels with BET surface areas of $280\text{ m}^2\text{ g}^{-1}$.^[17] The similar characteristics of aerogels from CellNFs^[18] and CNTs^[19] are $20\text{--}284\text{ m}^2\text{ g}^{-1}$ and $184\text{ m}^2\text{ g}^{-1}$, respectively.

The special ability of BANF to form 3DNs can be appreciated from wet-spinning experiments (Supporting Information, Figure S3b, Video S2). A 0.1% (w/v) BANF dispersion is extruded from a needle with inner diameter of $180\text{ }\mu\text{m}$ into a flow of DI water. It is observed that the fluid BANF dispersion quickly transformed into continuous hydrogel fibers (Figure 2g,h). Owing to the fluorescence of PPTA (Supporting Information, Figure S4), the BANF fibers show green luminescence under UV light (Supporting Information, Video S3). Notably, the extruded hydrogel fibers have a diameter of $172 \pm 15\text{ }\mu\text{m}$, which is identical within experimental error to the inner diameter of the needle, and does not change after supercritical drying (Supporting Information, Figure S3c). These properties should be attributed to the resistance of the 3DNs constructed from BANFs to capillary pressure.

An SEM image of the internal part of the fiber (Supporting Information, Figure S3d) confirms its 3DN morphology; the porosity of the network is similar to that obtained by the diffusion process in Figure 2e. No other nanomaterials can form continuous hydrogel fibers this way by themselves without resorting to other binding polymers^[20] or using high volumetric concentrations of nanofibers in the extrudant.^[21] For comparison, CellNFs cannot form continuous fibers^[5c] in a similar process (although it could potentially be done with a more intricate fiber making process stimulating CellNF alignment and mutual adhesion), even when the concentration of CellNFs was an order of magnitude higher, that is, 1% (w/v). Furthermore, long aging periods ($> 16\text{ h}$) are often necessary for obtaining stable CellNF 3DNs.^[5c]

The significance of branching can also be seen from the shear stress–strain curve of BANF hydrogels, which shows a linear viscoelastic region ending at a strain amplitude of 10%, followed by a softening region where the hydrogel starts to break and flow (Figure 3a). The maximum stress at the turning point, known as the critical shear strength, τ_c , is equal to $2.95 \pm 0.05\text{ kPa}$, which is much larger than that of graphene hydrogels ($\tau_c = 0.4\text{ kPa}$) at a similar solid content.^[3a]

The dynamic shear test helps us separate the elastic and viscous contributions to energy dissipation. The term of storage modulus, G' , characteristic of the elasticity of the gel, is, as expected from Figure 3a, constant for small strains, and then decreases for strains above 10% (Figure 3b). The loss modulus, G'' , initially increases and then decreases, which reflects structural rearrangement in the materials for strains above 10%. G' varies little with the angular frequency from 0.06 to 60 rad s^{-1} remaining around 29 kPa at a fixed oscillatory strain of 1% (Figure 3c). By contrast, G'' exhibits a region with a larger value at higher and lower frequency regions. The low frequency rise implies the existence of a slow structural rearrangement process, while the high frequency

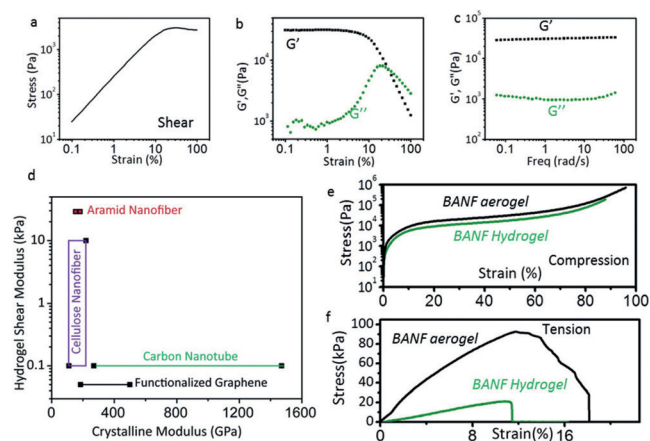


Figure 3. Mechanical properties of BANF hydrogels and aerogels. a) Oscillatory shear strain–stress curve of BANF hydrogels. b) Dependence of elastic moduli (G') and loss moduli (G'') on the strain amplitude. c) Dependence of G' and G'' on the frequency of the oscillatory shear. d) Comparison between BANF hydrogel and other high-crystalline-modulus nanomaterial hydrogels. The related data and references are listed in the Supporting Information, Table S1. e) Compressive stress–strain curves for BANF hydrogels and aerogels. f) Tensile stress–strain curves for BANF hydrogels and aerogels.

rise is attributed to the viscous relaxation of water in the hydrogel.

It can be seen that 1 wt% BANF hydrogels are much stiffer than hydrogels with similar or much higher solid content (Supporting Information, Table S1). They are also stiffer than circa 1 wt% hydrogels made from nanofibers and other rod-like nanoscale materials,^[22] indicating substantially better 3DN connectivity and stronger fiber-to-fiber contacts for BANFs (Figure 3d). Carbon nanotube or graphene hydrogels are generally weaker than those from BANF. Moreover, BANF hydrogels have three times higher G' than CellNF hydrogels (Supporting Information, Table S1).

Uniaxial deformation tests of the BANF hydrogels and aerogels indicate their high compressive and tensile strengths (Figure 3e,f; Supporting Information, Tables S2 and S3).^[2a,3b,18b] 3DNs from BANFs retain physical integrity after being compressed by 90% of the original size without introducing any cracks at the macro-, micro-, or nanoscale (Supporting Information, Figure S5a–f). At the same time, graphene or CellNF networks develop macroscopic cracks at strains of about 45% or 65%.^[3a,18a] The compressed aerogel shows increased mechanical properties under tension due to reduced porosity and the absence of cracks (Supporting Information, Figure S5h).

BANF 3DNs can also be used as frameworks for hosting polymer components to create novel nanocomposites. This can be done by allowing suitable polymers of choice to diffuse into BANF aero/hydrogels.^[5c] The interconnectivity of BANF aerogels can be transferred, in this way, directly to the hybrid materials. Polyvinyl alcohol (PVA) was selected as the example due to its abundant hydroxy groups capable of hydrogen-bonding with BANFs. BANF hydrogels (Supporting Information, Figure S6a) were fully wetted by a 1 wt% solution of PVA in water. $1.25\text{ }\mu\text{m}$ -thick translucent PVA/

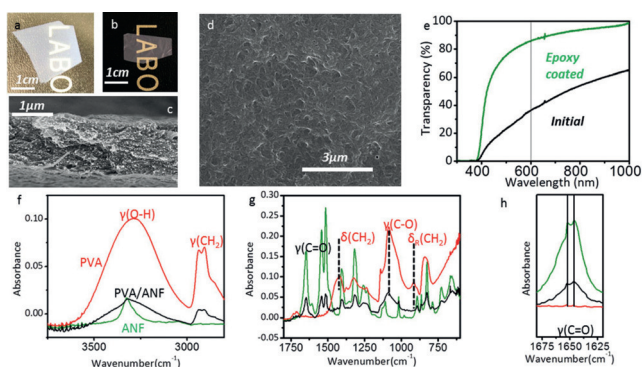


Figure 4. Fabrication and characterization of PVA/BANF composites. a) BANF hydrogel sheet floating in water. b) PVA/BANF composite film. c) Cross-section of the PVA/BANF composite film. d) Surface morphology of the PVA/BANF composite film. e) Transparency of PVA/BANF composite film with and without epoxy coating. f–h) FTIR spectra of PVA, BANF, and PVA/BANF composites. The stretching and bending modes of different functional groups are indicated by γ and δ , respectively.

BANF composite films with uniform BANF distribution were then obtained by drying the PVA-saturated hydrogels at 70 °C (Figure 4 a–c). The BANF content in the densified composite is about 35 wt % as determined by thermogravimetric analysis (Supporting Information, Figure S6b) and differential scanning calorimetry (Supporting Information, Figure S6c). Additional surface coatings by epoxy resins^[23] can further smooth the rough film surface (Figure 4d) and improve the transparency of the film to 86 % at 600 nm (Figure 4e).

The strong interactions between BANF and PVA were confirmed by FTIR (Figures 4 f–h). The presence of hydrogen bonds is evident from the change in the energy of $\gamma(\text{C}=\text{O})$ vibrations. The band at 1646 cm^{-1} for C=O associated with intra-nanofiber hydrogen bonds did not change appreciably, but the other C=O band for inter-nanofiber hydrogen bonds was upshifted by 0.8 cm^{-1} (Figure 4h). This observation suggests that OH groups from PVA compete with C=O groups as hydrogen acceptors, thus increasing the electron density on the C=O unit. The bending $\delta(\text{CH}_2)$ and rocking modes $\delta_{\text{R}}(\text{CH}_2)$ of $-\text{CH}_2-$ groups disappear in the FTIR spectra of BANF-PVA composites^[24] because strong van der Waals interactions from the phenylene groups of BANFs constrain the vibrations of $-\text{CH}_2-$ units in PVA.

The PVA/BANF composites showed ultimate strength and strain of $\sigma_u = 257 \pm 9$ MPa and $s_u = 27 \pm 5$ %, respectively (Supporting Information, Figure S7a). The mechanical properties of PVA/BANF films are comparable to or surpass the properties of the composites described previously (see the Supporting Information for more details).^[25] Along with the mechanical enhancement, the inclusion of BANF in PVA can significantly tune the coefficient of thermal expansion (CTE) of the composites, thanks to the negative CTE of BANF in the axial direction (see the Supporting Information and Figure S7b for more details).^[26]

In conclusion, BANFs stand out from other nanofibers by their extensive branching. This unusual geometry of nanofibers translates into the ability to form sparsely filled yet tightly interconnected networks due to entanglement of

flexible branches. The ability of 3DNs prepared from BANFs to distribute local stress and withstand capillary pressure opens the possibility to make a variety of hybrid materials combining BANF hydro- and aerogels with nanoparticles. As a potentially biocompatible material,^[27] BANFs could also find medical applications as durable scaffolds to address challenges in tissue engineering.

Acknowledgements

We are grateful to Michelle Gonzales and Thomas Rudolph for help with development of selected synthetic protocols. This study was partially supported by the Center for Solar and Thermal Energy Conversion, an Energy Frontier Research Center funded by the U.S. Department of Energy, Office of Science, Office of Basic Energy Sciences under Award Number DE-SC0000957. We acknowledge support from NSF under grant ECS-0601345; EFRI-BSBA 0938019; CBET 0933384; CBET 0932823; and CBET 1036672. The work is also partially supported by AFOSR MURI 444286-P061716 and NIH 1R21CA121841-01A2. This research was supported by NSF DMR-9871177 and DMR-0315633 grants. M.Y. thanks the financial support from the National Natural Science Foundation of China (Grant No. 21571041). The EMAL facilities at the University of Michigan are also acknowledged. The authors would like to particularly thank Hao Chen and Prof. Ralph T. Yang for their help in measuring the BET surface area of the BANF aerogels.

Conflict of interest

N.A.K. declares the conflict of interests as a co-founder of a company Elegus Technologies commercializing layered composites of ANFs and BANFs.

Keywords: aramid nanofibers · branching · gels · mechanical properties · three-dimensional networks

How to cite: *Angew. Chem. Int. Ed.* **2017**, *56*, 11744–11748
Angew. Chem. **2017**, *129*, 11906–11910

- [1] a) L. Hu, D. S. Hecht, G. Gruner, *Nano Lett.* **2004**, *4*, 2513–2517; b) T. Ramanathan, A. A. Abdala, S. Stankovich, D. A. Dikin, M. Herrera Alonso, R. D. Piner, D. H. Adamson, H. C. Schniepp, X. Chen, R. S. Ruoff, S. T. Nguyen, I. A. Aksay, R. K. Prud'Homme, L. C. Brinson, *Nat. Nanotechnol.* **2008**, *3*, 327–331; c) P. Podsiadlo, A. K. Kaushik, E. M. Arruda, A. M. Waas, B. S. Shim, J. D. Xu, H. Nandivada, B. G. Pumplin, J. Lahann, A. Ramamoorthy, N. A. Kotov, *Science* **2007**, *318*, 80–83; d) S. Stankovich, D. A. Dikin, G. H. B. Dommett, K. M. Kohlhaas, E. J. Zimney, E. A. Stach, R. D. Piner, S. T. Nguyen, R. S. Ruoff, *Nature* **2006**, *442*, 282–286; e) M. Sahimi, *Applications of percolation theory*, Taylor & Francis Inc., Bristol, **1994**; f) N. C. Bigall, A. K. Herrmann, M. Vogel, M. Rose, P. Simon, W. Carrillo-Cabrera, D. Dorfs, S. Kaskel, N. Gaponik, A. Eychmuller, *Angew. Chem. Int. Ed.* **2009**, *48*, 9731–9734; *Angew. Chem.* **2009**, *121*, 9911–9915; g) J. L. Mohanan, I. U. Arachchige, S. L. Brock, *Science* **2005**, *307*, 397–400; h) C. Aulin, J. Netrval, L. Wagberg, T. Lindstrom, *Soft Matter* **2010**, *6*, 3298–3305; i) N.

- Gaponik, A. K. Herrmann, A. Eychmuller, *J. Phys. Chem. Lett.* **2012**, *3*, 8–17; j) D. Jang, L. R. Meza, F. Greer, J. R. Greer, *Nat. Mater.* **2013**, *12*, 893–898; k) B. L. Allen, P. D. Kichambare, A. Star, *Adv. Mater.* **2007**, *19*, 1439–1451; l) S. R. Ye, A. R. Rathmell, Z. F. Chen, I. E. Stewart, B. J. Wiley, *Adv. Mater.* **2014**, *26*, 6670–6687; m) M. F. L. De Volder, S. H. Tawfick, R. H. Baughman, A. J. Hart, *Science* **2013**, *339*, 535–539; n) V. Sayevich, B. Cai, A. Benad, D. Haubold, L. Sonntag, N. Gaponik, V. Lesnyak, A. Eychmuller, *Angew. Chem. Int. Ed.* **2016**, *55*, 6334–6338; *Angew. Chem.* **2016**, *128*, 6442–6446.
- [2] a) M. A. Worsley, S. O. Kucheyev, J. H. Satcher, A. V. Hamza, T. F. Baumann, *Appl. Phys. Lett.* **2009**, *94*, 073115; b) L. A. Hough, M. F. Islam, B. Hammouda, A. G. Yodh, P. A. Heiney, *Nano Lett.* **2006**, *6*, 313–317; c) M. B. Bryning, D. E. Milkie, M. F. Islam, L. A. Hough, J. M. Kikkawa, A. G. Yodh, *Adv. Mater.* **2007**, *19*, 661–664; d) S. Ozden, C. S. Tiwary, A. H. C. Hart, A. C. Chipara, R. Romero-Aburto, M. T. F. Rodrigues, J. Taha-Tijerina, R. Vajtai, P. M. Ajayan, *Adv. Mater.* **2015**, *27*, 1842–1850.
- [3] a) Y. X. Xu, K. X. Sheng, C. Li, G. Q. Shi, *ACS Nano* **2010**, *4*, 4324–4330; b) H. Y. Sun, Z. Xu, C. Gao, *Adv. Mater.* **2013**, *25*, 2554–2560.
- [4] a) E. C. Garnett, W. S. Cai, J. J. Cha, F. Mahmood, S. T. Connor, M. G. Christoforo, Y. Cui, M. D. McGehee, M. L. Brongersma, *Nat. Mater.* **2012**, *11*, 241–249; b) B. Yeom, T. Sain, N. Laceyvic, D. Bukharina, S.-H. Cha, A. M. Waas, E. M. Arruda, N. A. Kotov, *Nature* **2017**, *543*, 95–98.
- [5] a) B. Wicklein, A. Kocjan, G. Salazar-Alvarez, F. Carosio, G. Camino, M. Antonietti, L. Bergstrom, *Nat. Nanotechnol.* **2015**, *10*, 277–283; b) R. T. Olsson, M. A. S. A. Samir, G. Salazar-Alvarez, L. Belova, V. Strom, L. A. Berglund, O. Ikkala, J. Noguez, U. W. Gedde, *Nat. Nanotechnol.* **2010**, *5*, 584–588; c) J. R. Capadona, O. Van Den Berg, L. A. Capadona, M. Schroeter, S. J. Rowan, D. J. Tyler, C. Weder, *Nat. Nanotechnol.* **2007**, *2*, 765–769; d) Y. Kobayashi, T. Saito, A. Isogai, *Angew. Chem. Int. Ed.* **2014**, *53*, 10394–10397; *Angew. Chem.* **2014**, *126*, 10562–10565.
- [6] a) J. Zhao, J.-W. Jiang, Y. Jia, W. Guo, T. Rabczuk, *Carbon* **2013**, *57*, 108–119; b) Y. Ye, C. C. Ahn, C. Witham, B. Fultz, J. Liu, A. G. Rinzler, D. Colbert, K. A. Smith, R. E. Smalley, *Appl. Phys. Lett.* **1999**, *74*, 2307–2309.
- [7] *Physical properties of polymers handbook*, 2nd ed., Springer, New York, **2006**.
- [8] J. G. Torres-Rendon, F. H. Schacher, S. Ifuku, A. Walther, *Biomacromolecules* **2014**, *15*, 2709–2717.
- [9] J. P. F. Lagerwall, C. Schutz, M. Salajkova, J. Noh, J. Hyun Park, G. Scalia, L. Bergstrom, *NPG Asia Mater.* **2014**, *6*, e80.
- [10] L. Blanchoin, K. J. Amann, H. N. Higgs, J. B. Marchand, D. A. Kaiser, T. D. Pollard, *Nature* **2000**, *404*, 1007–1011.
- [11] D. A. Fletcher, D. Mullins, *Nature* **2010**, *463*, 485–492.
- [12] a) T. Pujol, O. du Roure, M. Fermigier, J. Heuvingh, *Proc. Natl. Acad. Sci. USA* **2012**, *109*, 10364–10369; b) M. L. Gardel, J. H. Shin, F. C. MacKintosh, L. Mahadevan, P. Matsudaira, D. A. Weitz, *Science* **2004**, *304*, 1301–1305; c) C. P. Broedersz, F. C. MacKintosh, *Rev. Mod. Phys.* **2014**, *86*, 995–1036.
- [13] a) F. C. Mackintosh, J. Kas, P. A. Janmey, *Phys. Rev. Lett.* **1995**, *75*, 4425–4428; b) K. I. Sano, R. Kawamura, T. Tominaga, N. Oda, K. Ijiro, Y. Osada, *Biomacromolecules* **2011**, *12*, 4173–4177.
- [14] a) M. Yang, K. Cao, L. Sui, Y. Qi, J. Zhu, A. Waas, E. M. Arruda, J. Kieffer, M. D. Thouless, N. A. Kotov, *ACS Nano* **2011**, *5*, 6945–6954; b) J. Q. Zhu, W. X. Cao, M. L. Yue, Y. Hou, J. C. Han, M. Yang, *ACS Nano* **2015**, *9*, 2489–2501; c) S. O. Tung, S. Ho, M. Yang, R. Zhang, N. A. Kotov, *Nat. Commun.* **2015**, *6*, 6152.
- [15] a) R. N. Jones, C. L. Angell, T. Ito, R. J. D. Smith, *Can. J. Chem.* **1959**, *37*, 2007–2022; b) E. M. Krauss, S. I. Chan, *J. Am. Chem. Soc.* **1982**, *104*, 1824–1830.
- [16] L. R. Meza, S. Das, J. R. Greer, *Science* **2014**, *345*, 1322–1326.
- [17] Y. Zhao, C. Hu, Y. Hu, H. Cheng, G. Shi, L. Qu, *Angew. Chem. Int. Ed.* **2012**, *51*, 11371–11375; *Angew. Chem.* **2012**, *124*, 11533–11537.
- [18] a) M. Pääkkö, J. Vapaavuori, R. Silvennoinen, H. Kosonen, M. Ankerfors, T. Lindstrom, L. A. Berglund, O. Ikkala, *Soft Matter* **2008**, *4*, 2492–2499; b) H. Sehaqui, M. Salajkova, Q. Zhou, L. A. Berglund, *Soft Matter* **2010**, *6*, 1824–1832; c) H. Sehaqui, Q. Zhou, L. A. Berglund, *Compos. Sci. Technol.* **2011**, *71*, 1593–1599.
- [19] M. A. Worsley, S. O. Kucheyev, J. D. Kuntz, A. V. Hamza, J. H. Satcher, T. F. Baumann, *J. Mater. Chem.* **2009**, *19*, 3370–3372.
- [20] L. M. Ericson, H. Fan, H. Q. Peng, V. A. Davis, W. Zhou, J. Sulpizio, Y. H. Wang, R. Booker, J. Vavro, C. Guthy, A. N. G. Parra-Vasquez, M. J. Kim, S. Ramesh, R. K. Saini, C. Kittrell, G. Lavin, H. Schmidt, W. W. Adams, W. E. Billups, M. Pasquali, W. F. Hwang, R. H. Hauge, J. E. Fischer, R. E. Smalley, *Science* **2004**, *305*, 1447–1450.
- [21] I. Karadagli, B. Schulz, M. Schestakow, B. Milow, T. Gries, L. Ratke, *J. Supercrit. Fluids* **2015**, *106*, 105–114.
- [22] a) X. Wu, R. Moon, A. Martini, *Cellulose* **2013**, *20*, 43–55; b) K. Tashiro, M. Kobayashi, H. Tadokoro, *Macromolecules* **1977**, *10*, 413–420; c) C. Lee, X. D. Wei, J. W. Kysar, J. Hone, *Science* **2008**, *321*, 385–388; d) J. T. Paci, T. Belytschko, G. C. Schatz, *J. Phys. Chem. C* **2007**, *111*, 18099–18111; e) J. T. Robinson, M. Zalalutdinov, J. W. Baldwin, E. S. Snow, Z. Wei, P. Sheehan, B. H. Houston, *Nano Lett.* **2008**, *8*, 3441–3445.
- [23] H. Yano, J. Sugiyama, A. N. Nakagaito, M. Nogi, T. Matsuura, M. Hikita, K. Handa, *Adv. Mater.* **2005**, *17*, 153–155.
- [24] S. Krimm, C. Y. Liang, G. B. B. M. Sutherland, *J. Polym. Sci.* **1956**, *22*, 227–247.
- [25] a) M. Nogi, S. Iwamoto, A. N. Nakagaito, H. Yano, *Adv. Mater.* **2009**, *21*, 1595–1598; b) H. Sehaqui, Q. Zhou, L. A. Berglund, *Soft Matter* **2011**, *7*, 7342–7350; c) L. J. Bonderer, A. R. Studart, L. J. Gauckler, *Science* **2008**, *319*, 1069–1073; d) B. S. Shim, J. Zhu, E. Jan, K. Critchley, S. S. Ho, P. Podsiadlo, K. Sun, N. A. Kotov, *ACS Nano* **2009**, *3*, 1711–1722.
- [26] J. Zhu, C. M. Andres, J. Xu, A. Ramamoorthy, T. Tsotsis, N. A. Kotov, *ACS Nano* **2012**, *6*, 8357–8365.
- [27] J. D. Henderson, R. H. Mullarky, D. E. Ryan, *J. Biomed. Mater. Res.* **1987**, *21*, 59–64.

Manuscript received: April 11, 2017

Revised manuscript received: July 11, 2017

Accepted manuscript online: July 18, 2017

Version of record online: August 18, 2017